Extreme ionization of Xe clusters driven by ultraintense laser fields

Andreas Heidenreich, Isidore Last, and Joshua Jortner
School of Chemistry, Tel-Aviv University, 69978 Tel-Aviv, Israel

(Received 6 June 2006; accepted 27 June 2007; published online 21 August 2007)

We applied theoretical models and molecular dynamics simulations to explore extreme multielectron ionization in Xe_n clusters ($n=2-2171$, initial cluster radius $R_0=2.16-31.0$ Å) driven by ultraintense infrared Gaussian laser fields (peak intensity $I_M=10^{15}-10^{20}$ W cm^{-2}, temporal pulse length $\tau=10-100$ fs, and frequency $\nu=0.35$ fs^{-1}). Cluster compound ionization was described by three processes of inner ionization, nanoplasma formation, and outer ionization. Inner ionization gives rise to high ionization levels (with the formation of $\{Xe^{q+}\}_n$ with $q=2-36$), which are amenable to experimental observation. The cluster size and laser intensity dependence of the inner ionization levels are induced by a superposition of barrier suppression ionization (BSI) and electron impact ionization (EII). The BSI was induced by a composite field involving the laser field and an inner field of the ions and electrons, which manifests ignition enhancement and screening retardation effects. EII was treated using experimental cross sections, with a proper account of sequential impact ionization. At the highest intensities ($I_M=10^{18}-10^{20}$ W cm^{-2}) inner ionization is dominated by BSI. At lower intensities ($I_M=10^{15}-10^{16}$ W cm^{-2}), where the nanoplasma is persistent, the EII contribution to the inner ionization yield is substantial. It increases with increasing the cluster size, exerts a marked effect on the increase of the $\{Xe^{q+}\}_n$ ionization level, is most pronounced in the cluster center, and manifests a marked increase with increasing the pulse length (i.e., becoming the dominant ionization channel (56%) for Xe_{2171} at $\tau=100$ fs). The EII yield and the ionization level enhancement decrease with increasing the laser intensity. The pulse length dependence of the EII yield at $I_M=10^{15}-10^{16}$ W cm^{-2} establishes an ultraintense laser pulse length control mechanism of extreme ionization products. © *2007 American Institute of Physics*. [DOI: 10.1063/1.2762217]

I. INTRODUCTION

Clusters constitute large, finite systems with a density comparable to that of the solid or liquid condensed phase.[1] The response of elemental and molecular clusters to near-infrared ultraintense laser fields (peak intensity $I_M=10^{15}-10^{20}$ W cm^{-2}, temporal width $\tau=10-100$ fs) drives novel ionization processes[2–33] and manifests new features of electron dynamics[2,3,7,8,16–18,21–24] on the time scale of $<1-100$ fs. The extreme multielectron ionization mechanism of clusters involves three processes of inner ionization, nanoplasma formation, and outer ionization.[2,3,10,11,16,17,21–23] Inner ionization results in the formation of a charged, energetic nanoplasma within the cluster or in its vicinity, which is followed by the partial or complete outer ionization of the nanoplasma.[2,3,10,11,16,17,21–23,26,29,32,33] Extreme multielectron ionization of elemental and molecular clusters, e.g., Ar_n,[3–7,37–40] Xe_n,[2,3,5,13,15,26,35,38] $(H_2)_n$,[41] $(D_2)_n$,[42–45] $(H_2O)_n$,[34,46] $(D_2O)_n$,[27,34] $(CH_4)_n$,[30] $(CD_4)_n$,[20,30,47] and $(HI)_n$,[46,48,49] leads to the production of highly charged ions or nuclei, e.g., H^+ and D^+,[7–9,11,20,22,23,30,50] O^{q+} $(q=6-8)$,[9,27,51] C^{q+} $(q=4-6)$,[20,24,30,34,47,51] and Xe^{q+} $(q=3-26)$.[3,15,16,21,22,26,29,33,52,53] Cluster multielectron ionization, nanoplasma dynamics and response were explored by theoretical models[2,3,6,7,16–18,21,23,32,33,36,38,54–57] and by computer simulations.[4,6,9,21–24,26,29,32,45,50,58,59] Microscopic models for the cluster inner ionization level were based on the barrier suppression ionization (BSI) model.[10,11,21,29,60] An additional contribution to cluster inner ionization arises from electron impact ionization (EII) induced by the high-energy (50 eV–1 M eV) nanoplasma electrons.[10,11,14,21,29]

Elemental Xe_n clusters constitute a benchmark system for experimental[5,13,15,35,52,61–69] and theoretical[2,3,9–11,16–18,21,22,26,29,33,38,53,70–73] studies in this field. In spite of these extensive explorations, the physical mechanisms underlying inner/outer ionization, nanoplasma response and electron dynamics, as well as Coulomb explosion dynamics, were not yet established. We applied microscopic models, together with molecular dynamics (MD) simulations, to provide information on multielectron inner ionization of Xe_n clusters driven by ultraintense, infrared laser pulses, focusing on the following mechanistic issues.

(1) The relative contributions of the BSI and of the EII mechanisms for inner ionization over a broad cluster size, laser intensity, and pulse length domains. In our previous work, the Lotz empirical equation for cross sections[74] was used[10,21,22,29] for estimates of EII in clusters. The empirical parameters initially used[10,21] in the Lotz equation were not reliable. Our recent work[29] allowed for the proper parametrization of the EII cross sections.[29,75] In the present work the EII molecular dynamics scheme previously given by us[29] will be modified, providing information on the EII ionization levels, on the total ionization levels, and on the nanoplasma population.

(2) Distinct intensity domain for inner ionization. Inner ionization levels for the highest intensities ($I_M = 10^{18}-10^{20}$ W cm^{-2}), which correspond to the relativistic region,[21] reveal qualitatively different features than for the lower intensities ($I_M = 10^{15}-10^{16}$ W cm^{-2}), where the EII process is significant.
Concurrently, some general features of cluster inner ionization were established.
(3) The spatial nonuniformity of the distribution of the charges $\{q\}$ of the multiple ionized Xe^{q+} ions was determined.
(4) The reactive EII dynamics of the nanoplasma electrons driven by the laser field and in the "laser-free" domain after the termination of the laser pulse was explored.
(5) Conditions for the control of the extreme ionization products in ultraintense laser fields,[25,26] which are driven by EII, were established.

In this paper we utilize MD simulations for high-energy electrons and ions[21,29] to study inner ionization mechanisms, extreme inner ionization levels, and reactive electron dynamics in Xe_n clusters ($n=2-2171$) driven by ultraintense Gaussian infrared laser pulses with peak intensities $I_M = 10^{15}-10^{20}$ W cm^{-2} (Secs. II and III). In Sec. IV we confront our computational results for long-time inner ionization levels with experimental data for the formation of extremely ionized $\{Xe^{q+}\}$ ions within the macroscopic plasma filament,[2–6] which is produced by Coulomb explosion of an assembly of clusters.[42–47]

II. MULTIELECTRON INNER IONIZATION

A. Methodology

The energetics and dynamics of the energetic electrons and of the multicharged ions in Xe_n clusters ($n=2-2171$ and initial cluster radii $R_0=2.16-31.0$ Å) were obtained from classical MD simulations for clusters driven by the ultraintense laser field.[21,29] In our simulations we have used initial closed spherical fcc structures of $(Xe^+)_n$ clusters, with a nearest-neighbor distance of 4.33 Å. The differences between these closed spherical fcc structures and the icosahedral closed shell structures of rare gases are insignificant in view of the strong ion-ion and electron-ion interactions. The ultraintense, Gaussian, infrared laser pulse was taken in the peak intensity range $I_M = 10^{15}-10^{20}$ W cm^{-2}, temporal pulse length $\tau = 10-100$ fs, and frequency $\nu = 0.35$ fs^{-1} (photon energy $h\nu = 1.44$ eV). An initially truncated Gaussian laser pulse was used with the initial laser field (corresponding to the production of singly charged ions and stripped electrons), being located at $t=t_s$ ($t_s<0$), whose laser intensity and pulse length dependence were described.[10,21,29] The composite electric field, which drives BSI processes,[10,16,21,29,56] is the superposition of the external laser field and the inner electrostatic field generated by all ions and by the nanoplasma electrons. In the calculation of the inner field, a cutoff radius $r_{BSI}=2.6$ Å was introduced for the electron-ion distance[21] in order to avoid the inclusion of spurious field ionization induced by closely located electrons. Each electron produced by the BSI was initially placed with zero kinetic energy at the BSI barrier of its Xe^{q+} parent ion.[21,29] Electron-ion recombination within the nanoplasma was neglected.[70] The MD code[21,29] included relativistic effects based on the solution of the relativistic equations of motion for the electrons, as well as laser magnetic field effects.[21] These contribute notably in the intensity range of $I_M \geqslant 10^{18}$ W cm^{-2}.[21] For the analysis of the trajectories in the Gaussian laser field (with an onset at t_s and pulse maximum at $t=0$), it is convenient to set the temporal "long-time" end of the laser pulse at $t=t_L$, where $t_L \gg -t_s$.

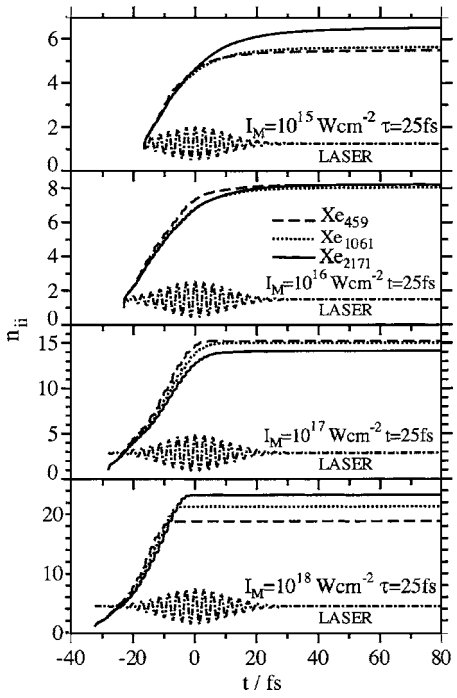

FIG. 1. The time dependence of the inner ionization levels n_{ii} (average charge q_{av} per atom) for Xe_n clusters ($n=459$, 1061, and 2171 as marked on the panels) for the intensities (a) $I_M = 10^{15}$ W cm^{-2}, (b) $I_M = 10^{16}$ W cm^{-2}, (c) $I_M = 10^{17}$ W cm^{-2}, and (d) $I_M = 10^{18}$ W cm^{-2}. The laser pulse width is $\tau = 25$ fs. The electric fields of the Gaussian laser pulses (-·---), expressed in arbitrary units for $t \geqslant t_s$, are represented on each panel, marked LASER.

B. Gross features of inner ionization

Figure 1 presents the simulation results for the time dependence of the inner ionization of Xe_n clusters ($n=459$, 1061, and 2171) interacting with Gaussian laser pulses ($\tau = 25$ fs) with peak intensities $I_M = 10^{15}$, 10^{16}, 10^{17}, and 10^{18} W cm^{-2}. The total number of electrons N_{ii} produced by inner ionization is

$$N_{ii} = N_{BSI} + N_{imp}, \tag{1}$$

where N_{BSI} is the total number of electrons produced by BSI and N_{imp} is the total number of electrons produced by EII. The inner ionization level n_{ii} per constituent atom is

$$n_{ii} = N_{ii}/n = n_{BSI} + n_{imp}, \tag{2}$$

where the BSI level (calculated using the procedure of Sec. II A) is $n_{BSI}=N_{BSI}/n$ and the EII level (calculated using the procedure of Sec. III below) is $n_{imp}=N_{imp}/n$. The time dependence of $n_{ii}(t)$, Fig. 1, reveals saturation or near saturation of the inner ionization level. At the termination of the

laser pulse at $t=-t_s$, $n_{ii}(-t_s)$ reaches near saturation at $I_M=10^{15}$ W cm^{-2} and saturation at $I_M=10^{17}$ and 10^{18} W cm^{-2}. This pattern is cluster size independent. The long-time inner ionization levels $n_{ii}^L \equiv n_{ii}(t_L)$ correspond to the final average charges of the $\{Xe^{q+}\}_n$ ions. These positive ions are amenable to experimental interrogation within the macroscopic nanoplasma,[2–6,59] which is produced by subsequent cluster outer ionization[2,3,10,21] and Coulomb explosion within an assembly of clusters.[42–47] The simulated values of n_{ii}^L (at $t_L \simeq 92$ fs) exhibit an irregular cluster size dependence at different values of I_M. n_{ii}^L increases with increasing n at $I_M=10^{15}$ and 10^{18} W cm^{-2}, being nearly cluster size independent at $I_M=10^{16}$ W cm^{-2}, and decreases with increasing n at $I_M=10^{17}$ W cm^{-2}. In what follows this pattern of n_{ii}^L will be attributed to the interplay between the contributions of the inner electric field (of the nanoplasma electrons and ions) to the BSI and of the EII to n_{ii}.

C. Inner ionization levels

Intensity and cluster size dependent multiple ionization of Xe_n clusters results in the production of $\{Xe^{q+}\}_n$ ions and is characterized by a distribution $\{q\}$ of the ionic charges. The inner ionization level, Eq. (2), is

$$n_{ii} = \sum_q n(q)q, \tag{3}$$

where $n(q)$ is the abundance of ions of charge q per Xe atom, with $\Sigma_q n(q)=1$. The inner ionization level $\equiv n_{ii}(t)$ (Fig. 1) and the charge distribution $n(q) \equiv n(q;t)$ are time dependent. The average charge per ion at long times is given by the asymptotic inner ionization level n_{ii}^L. n_{ii}^L is determined by (i) the laser field that makes the most important contribution to the composite (laser+inner) field, which drives BSI;[21,22,70,76] (ii) the laser pulse temporal length (and shape); (iii) the ignition effect,[16–18,21,26,76] which results in the enhancement of the inner field that contributes to BSI; (iv) the screening effect[21,22,32] induced by the contribution of the nanoplasma electrons to the inner field, which reduces the inner field; (v) the EII contributions.[21,29]

To provide a complete description of the cluster size and laser intensity dependence of the inner ionization level $n_{ii}^L = n_{BSI}^L + n_{imp}^L$, according to Eq. (2), further information is required concerning the interplay between the contributions of BSI (which can exhibit a laser field dominated inner ionization, whose contribution to n_{BSI}^L is independent of n), ignition (where n_{ii}^L increases with increasing n), screening (where n_{BSI}^L decreases with increasing n), and EII (see Sec. III). A contribution to the decrease of n_{BSI}^L with increasing n can also arise from competition between BSI and EII (Sec. III). In Fig. 2 we portray the cluster size dependence of the two distinct contributions n_{BSI}^L and n_{imp}^L to n_{ii}^L, together with the maximal ionic charge q_{max} in the cluster size domain of $n=2-2171$. From these results we conclude that:

(1) Ignition effects on n_{BSI}^L are manifested for very small Xe_n clusters ($n=2-13$) at the lowest intensity of $I_M=10^{15}$ W cm^{-2}, where n_{BSI}^L and n_{ii}^L markedly increase with increasing n [Fig. 2(a)]. In the small cluster size domain ($n=2-13$), n_{imp}^L is very small so that the dominating contribution to n_{ii}^L originates from the BSI (i.e., $n_{ii}^L = n_{BSI}^L$). The inner ionization level n_{ii}^L for Xe_2 and Xe_3 at a fixed spatial configuration exhibits spatial anisotropy, with the laser electric field parallel to the Xe–Xe axis resulting in higher values of n_{ii}^L ($=n_{BSI}^L$) than when the electric field is perpendicular to the Xe–Xe axis [Fig. 2(a)]. For these small clusters complete outer ionization takes place and the inner field $F^{(+)}$ originates from the contribution of the ion charges (q). For Xe_2 with $F^{(+)}$ being parallel to the Xe–Xe axis $F^{(+)}=\bar{B}q^2r_0^2 \simeq 1.3q^2$ eV Å^{-1} (where r_0 is the initial constituent radius). For $q=2$, $F^{(+)}=5.2$ eV Å^{-1}, which is comparable to the laser field $F_M=6.9$ eV Å^{-1} at the peak intensity $I_M=10^{15}$ W cm^{-2}. Similar estimates for Xe_3 and Xe_n ($n=4-13$) clusters rationalize the marked contribution of ignition effects for these small ($n=2-13$) clusters at the lowest intensity. To further explore the ionization mechanism of small Xe_n clusters, we followed Siedschlag and Rost[16,33] and simulated the ionization levels

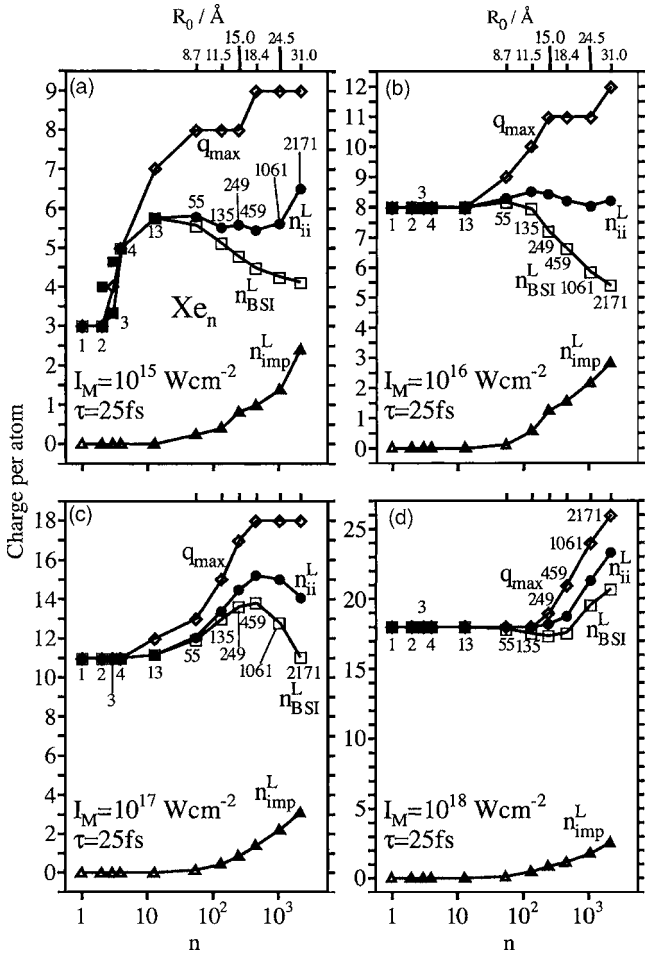

FIG. 2. The cluster size dependence of the long-time BSI level n_{BSI}^L (○), the EII level n_{imp}^L (△), the total inner ionization level n_{ii}^L (● and ■), and the maximal ionic charge q_{max} (◇) from Xe_n($n=1-2171$). All these long-time ionization levels are given per atom. n_{ii}^L gives the average charge of the Xe^{q+} ions, with the partial contribution of n_{BSI}^L and n_{imp}^L. (a) $I_M=10^{15}$ W cm^{-2} ($\tau=25$ fs). The $n_{BSI}^L=n_{ii}^L$ data for small ($n=2$ and 3) clusters at a fixed nuclear configuration are dependent on the direction of the laser field, with (■) for the laser field being parallel to the molecular axis and (●) for the laser field being perpendicular to the molecular axis. (b) $I_M=10^{16}$ W cm^{-2} ($\tau=25$ fs), (c) $I_M=10^{17}$ W cm^{-2} ($\tau=25$ fs), and (d) $I_M=10^{18}$ W cm^{-2} ($\tau=25$ fs).

of Xe_{13} at fixed nuclear configurations, using our computational scheme with the laser parameters $I_M=9\times10^{14}$ W cm^{-2}, $\tau=50$ fs, and $\nu=0.35$ fs^{-1}. Our simulations showed that the inner ionization level n_{ii}^L decreases monotonously with increasing the internuclear distance. On the other hand, the outer ionization level at $t=t_L$ exhibits a maximum in the outer ionization level at fixed nuclei, in accord with the results of Siedschlag and Rost.[16,33] We note that the inner ionization level simulated herein pertains to the relevant experimental observable (Sec. II B). Siedschlag and Rost[16,33] interpreted their results by the molecular enhanced ionization mechanism.[77–79] In the cluster ionization model used in Ref. 16 and 33, and also in the present work, quantum valence effects[77–79] are absent. A further exploration of these issues is called for.

(2) No ignition effects are manifested for small Xe_n ($n=2-13$) clusters in the higher intensity range of $I_M=10^{16}$ W cm^{-2} [Fig. 2(b)], $I_M=10^{17}$ W cm^{-2} [Fig. 2(c)], and $I_M=10^{18}$ W cm^{-2} [Fig. 2(d)]. In the higher intensity range of $I_M\geqslant10^{16}$ W cm^{-2}, the laser electric field at the pulse peak is $F_M\geqslant27.5$ eV Å^{-1}, whereupon $F_M>F^{(+)}$, with the composite (laser+inner) field F, being dominated by the laser field for these small clusters. At $I_M\geqslant10^{16}$ W cm^{-2} and in the cluster size domain where $n_{imp}^L\ll n_{BSI}^L$, we observe that n_{ii}^L ($=n_{BSI}^L$) is nearly cluster size independent in the range $n=2-13$ at $I_M=10^{16}-10^{17}$ W cm^{-2} and in the broad range $n=2-135$ at $I_M=10^{18}$ W cm^{-2}.

(3) Ignition effects for larger ($n>55$) clusters are exhibited in the intensity domain $I_M=10^{17}-10^{18}$ W cm^{-2} [Figs. 2(c) and 2(d)]. At $I_M=10^{17}$ W cm^{-2}, n_{BSI}^L monotonously increases with increasing n in the range $n=13-459$, and at $I_M=10^{18}$ W cm^{-2} [Fig. 2(d)] n_{BSI}^L increases with increasing n in the range $n=459-2171$.

(4) Screening effects are exhibited for larger $n\geqslant13$ clusters in the lower intensity domain of $I_M=10^{15}-10^{16}$ W cm^{-2} [Figs. 2(a) and 2(b)], being manifested by the monotonous decrease of n_{ii}^L with increasing n in the range $n=135-1061$. At $I_M=10^{17}$ W cm^{-2} [Fig. 2(c)] screening effects prevail for $n=459-2171$, while at $I_M=10^{18}$ W cm^{-2} screening is not operative [Fig. 2(d)].

(5) The contribution of EII (see Sec. III) to inner ionization [Figs. 2(a)–2(d)] is significant (i.e., $n_{imp}^L\geqslant0.5$) for larger clusters ($n\geqslant55$). In the lower intensity range of $I_M=10^{15}-10^{16}$ W cm^{-2} [Figs. 2(a) and 2(b)], n_{ii}^L is nearly cluster size independent for $n=13-1061$, with the increase of n_{imp}^L compensating for the decrease due to screening effects (see Sec. III) in this size domain. The additional increase of n_{ii}^L between $n=1061$ and $n=2171$ at $I_M=10^{15}$ W cm^{-2} manifests EII. A similar pattern of the increasing of n_{ii}^L with increasing the cluster size, which was attributed to EII, was reported[70] for moderately low intensities of $I_M=10^{16}$ W cm^{-2} at a longer pulse length ($\tau=75$ fs) than used herein. At the intensity of $I_M=10^{18}$ W cm^{-2}, the increase of n_{ii}^L with increasing n in the range $n=249-2179$ originates from the enhancement of the BSI and the EII yields. The more complex pattern at $I_M=10^{17}$ W cm^{-2} [Fig. 2(c)] manifests ignition (at $n=55-459$) and screening ($n=459-2171$) contributions with an additional increase of n_{ii}^L due to EII.

(6) The distribution $n(q)$ of the charges of the Xe^{q+} ions is characterized by the average charge $q_{av}(=n_{ii}^L)$ and the maximal charge q_{max} [Figs. 2(a)–2(d)]. In some cases closed shell ions are produced. At $I_M=10^{15}$ W cm^{-2}, q_{max} flattens off ($n=55-459$), revealing the formation of the $\cdots4s^24p^64d^{10}$ closed shell Xe^{8+} ion, exhibiting a further increase for $n=2171$ due to EII, while at $I_M=10^{17}$ W cm^{-2} q_{max} flattens off ($n=459-2171$) at $q_{max}=18$, revealing the formation of the $\cdots3d^{10}4s^24p^6$ closed shell Xe^{18+} ion.

(7) The temporal evolution of the distribution of ionic charges manifests a marked intensity dependence. The distribution $\{n(q)\}$ of the Xe^{q+} ion charges (per constituent atom) from a large Xe_{2171} cluster is rather broad, spanning a range Δq of the q values [Figs. 3(a) and 3(b)] of $\Delta q\simeq4-6$ at $I_M=10^{15}$ W cm^{-2} (for $t=15-110$ fs) and a range of q values of $\Delta q\simeq5-15$ at $I_M=10^{18}$ W cm^{-2} (for $t=10-125$ fs). At $I_M=10^{18}$ W cm^{-2} (where the BSI contribution dominates) a very broad charge distribution is manifested at intermediate times $(t-t_s)=15-25$ fs, which is due to a marked radial inhomogeneity of the ionic charges, with ignition effects being operative on the exterior cluster shells. Subsequent narrowing of $\{n(q)\}$ is then exhibited resulting in long-time distribution with $\Delta q\simeq7$ [Fig. 3(b)]. In the lower intensity region of $I_M=10^{15}$ W cm^{-2} (where EII contributions are appreciable, see Sec. III), the distribution $\{n(q)\}$ at $\tau=25$ fs is narrower with Δq being nearly time independent. The long-time distribution spans the range $q=5-9$ [Fig. 3(a)].

Figure 4 presents the radial distributions $n(q,r)$ of the Xe^{q+} ions of charge q at distance r from the center of the Xe_{2171} cluster, which are formed at the peak ($t=0$) and at the end ($t=-t_s$) of the laser pulses for $I_M=10^{15}$ W cm^{-2} ($\tau=25$ and 100 fs) and for $I_M=10^{18}$ W cm^{-2} ($\tau=25$ fs). The radial distribution was presented for intervals of $\Delta r/R=0.05$ and obey the normalization condition $\Sigma_r n(q,r)\Delta r=n(q)$. Most interesting are the data at $I_M=10^{15}$ W cm^{-2}, where the persistent nanoplasma exists. For Xe_{2171} at $I_M=10^{15}$ W cm^{-2} and $\tau=25$ fs, the largest values of $q=6-8$ that appear at $t=0$ are exhibited for the exterior cluster shells [upper panel on Fig. 4(a)], where ignition effects are significant. The cutoff of the ion distribution occurs at $r=33$ Å, which is close to the cluster radius $R_0=31.0$ Å, so that the cluster expansion parameter $R(t=0)/R_0=1.06$, indicating negligible Coulomb explosion under these conditions, where the persistent nanoplasma significantly contributes to the screening of interionic repulsions.[21,22,32] For Xe_{2171} at $I_M=10^{15}$ W cm^{-2} and $\tau=100$ fs [middle panel on Fig. 4(a)], the contribution of the high charge $q=8$ is again dominant near the cluster boundary, manifesting ignition effects, while a small amount of the higher charge $q=9$ is produced in the cluster due to EII induced by this long pulse length (see Sec. III). The cutoff of

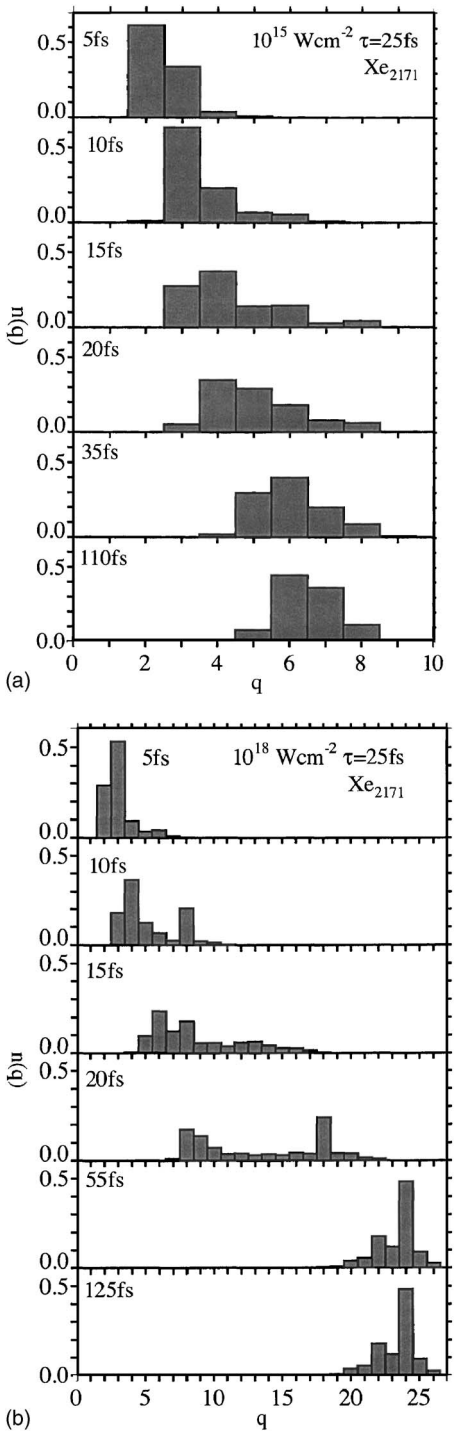

FIG. 3. The time-dependent distribution of the ionic charges $n(q)$ of $(Xe^{q+})_n$ ions at times $t-t_s=5-125$ fs (with the times marked on the panels) created by the inner ionization of Xe_{2171} clusters with a Gaussian laser pulse ($\tau=25$ fs) at intensities of $I_M=10^{15}$ W cm^{-2} (a) and $I_M=10^{18}$ W cm^{-2} (b).

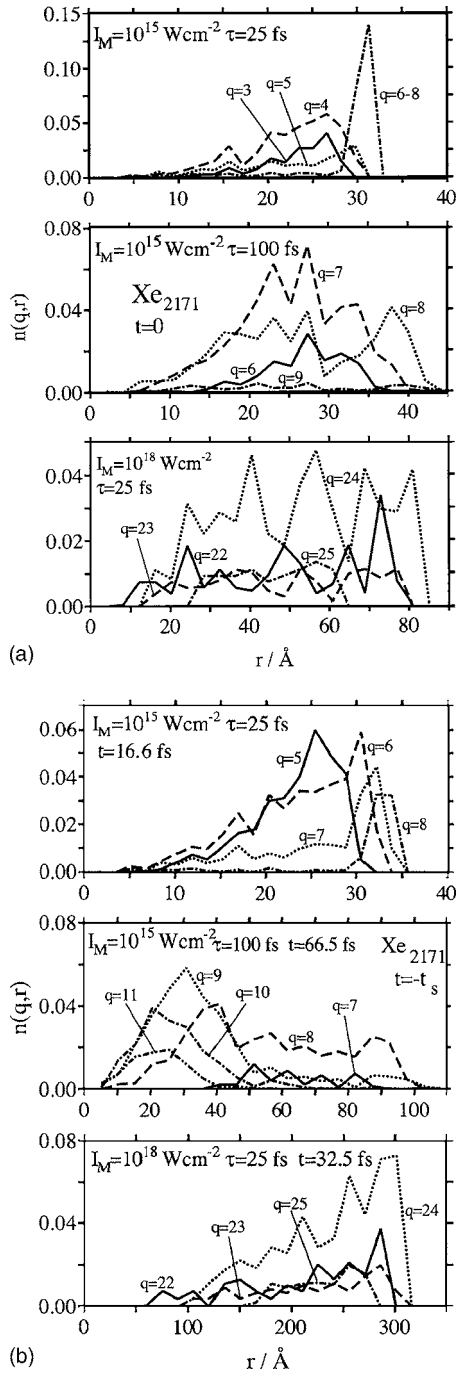

FIG. 4. The radial distribution $n(q,r)$ of Xe^{q+} ions at distances $r\cdots r+\Delta r$ ($\Delta r=R(t)/20$) from the cluster center. The ionic charges q are marked on the curves. The ions are produced by laser pulses of intensities $I_M=10^{15}$ W cm^{-2} and $I_M=10^{18}$ W cm^{-2} with pulse lengths of $\tau=25$ and 100 fs. The input data I_M and τ are labeled on each panel. The distributions of the individual ions are interrogated at time t. (a) $t=0$, corresponding to the peak of the laser pulse. (b) $t=-t_s$, corresponding to the termination of the laser pulse.

the ion distribution at $I_M=10^{15}$ W cm^{-2} and $\tau=100$ fs [middle panel of Fig. 4(a)] is exhibited at $R(t=0)\simeq 45$ Å, with an expansion parameter $R(t=0)/R_0=1.45$, revealing the onset of Coulomb explosion at $t=0$ for this "long" pulse. Moving from the pulse peak ($t=0$) to the pulse end ($t=-t_s$), the radius of the Xe_{2171} cluster at $I_M=10^{15}$ W cm^{-2} and $\tau=25$ fs slightly increases to the edge value $R(t-t_s)=36$ Å [upper panel of Fig. 4(b)] so that $R(t=-t_s)/R_0=1.16$, manifesting the onset of Coulomb explosion. Concurrently, effects of EII are manifested for $I_M=10^{15}$ W cm^{-2} ($\tau=25$ fs) with the population of the higher charges $q=5-8$ at $t=0$ and $t=-t_s$ [upper panels in Figs. 4(a) and 4(b)]. Dramatic effects of EII are manifested at $t=-t_s$ for $I_M=10^{15}$ W cm^{-2} and $\tau=100$ fs, where higher charges of $q=9-11$ are generated, with their distribution peaks inside the cluster [central panel on Fig. 4(b)]. For this long pulse length, the contribution of the EII to the inner ionization yield is significant, manifest-

ing the formation of large charges (see Sec. III). The charge distribution at $t=-t_s$ for $\tau=100$ fs [Fig. 4(b), middle panel] reveals that EII by the persistent nanoplasma is important in the central part of the cluster. At $t=-t_s$ for $\tau=100$ fs, Coulomb explosion sets in where the cutoff of the ion distribution gives $R(t=-t_s)=105$ Å, i.e., $R(t=-t_s)/R_0=3.18$ [middle panel of Fig. 4(b)]. Under these conditions EII and Coulomb explosion take place on the same time scale.

For the high intensity of $I_M=10^{18}$ W cm^{-2} ($\tau=25$ fs) at $t=0$, the large charges of $q=22-25$ are spread throughout the cluster [lower panel in Fig. 4(a)] and already exhibit appreciable Coulomb explosion, i.e., $R(t=0)/R_0=2.8$, which is due to a high ionization level and to effective outer ionization of the transient nanoplasma. There is no radial charge ordering at $t=0$ and at $t=-t_s$ [lower panels in Figs. 4(a) and 4(b)], as the composite field on the outer shell was decreased due to Coulomb explosion. At the end of the pulse ($t=-t_s$), appreciable Coulomb explosion is manifested [lower panel of Fig. 4(b)], with $R(t=-t_s)=320$ Å, i.e., $R(t=-t_s)/R_0\simeq 10$. At $I_M=10^{18}$ W cm^{-2}, the charge distribution in the range $q=22-25$ is invariant at $t=-t_s$, relative to $t=0$, revealing that in this high intensity the effect of EII is minor.

III. ELECTRON IMPACT IONIZATION

A. Treatment of EII

In our simulations we have included single EII processes $Xe^{q+}+e\rightarrow Xe^{(q+1)+}+2e$ for the formation of the nanoplasma. Experimental data for electron impact cross sections $\sigma_q(E)$, as functions of the impact energy E, are available up to $q=10$.[75] We have fitted[29] the experimental data[75] to a simplified version of the Lotz formula.[74] The treatment of EII rests on a stepwise sequential one-electron scheme.[29] EII was considered if a particular electron approaches an ion at a distance closer than 2 Å, with the occurrence of EII being checked for all electrons at each electronic time step (0.5–1 as). The simulations of EII were performed using the scheme advanced by us,[21,29] which was modified to account properly for the avoidance of spurious multiple ionization. After EII, the impinging and the ejected electrons are excluded by the simulation algorithm from further impact ionizations at the same parent ion, as long as they are inside the distance of approach of 2 Å for impact ionization. In this way, multiple impact ionizations are ruled out. In our previous simulations,[29] the algorithm for the avoidance of multiple ionizations was unsatisfactory, precluding further impact ionizations at an ion, even if an EII attempt was unsuccessful. While the impact ionization yields reported in our recent paper[29] were larger by roughly a numerical factor of ~2, as compared with the results of an older simulation[21] in which the electron impact cross sections were treated in a much more approximate way, these impact ionization yields[29] were still smaller by a numerical factor of ~2 as compared with the results reported in the present work (see Sec. III B) because of the unsatisfactory avoidance of multiple impact ionizations in our previous work.[29] We note in passing that the effects of electron-ion recollision including $(e,2e)$ processes[80–83] are intrinsically included in our treatment of impact ionization. These effects of electron-ion recollisions are of considerable importance at lower intensities ($I_M=10^{15}$ W cm^{-2}), where electron tunneling effects in the BSI (Ref. 84) have to be incorporated as well.

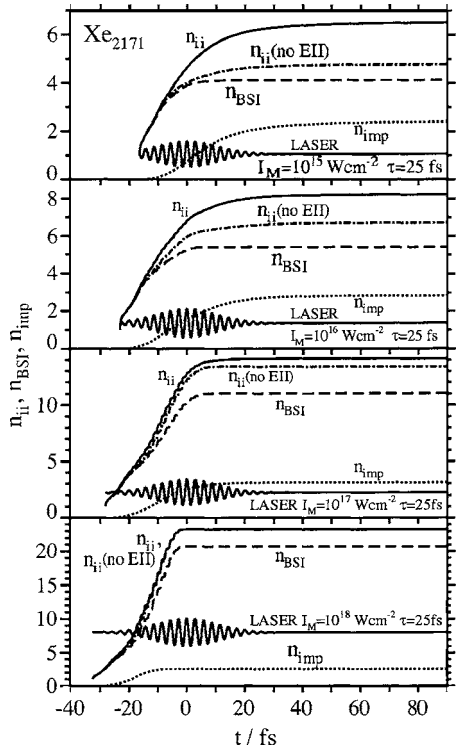

FIG. 5. The effect of EII on the inner ionization level, presenting the time dependence of the BSI level n_{BSI} (---), the EII level n_{imp} (···), and the n_{ii} level (—). These data are compared with the time dependent inner ionization levels in a model system where the EII channel is switched off, marked n_{ii} (without EII) (-·-·-). The data are for Xe_{2171} clusters at $I_M=10^{15}-10^{18}$ W cm^{-2} ($\tau=25$ fs) with the intensities marked on the panels. The laser field (solid line, marked LASER) is presented in arbitrary units.

B. EII yields

The EII data provide significant new information on the cluster size and laser parameter dependence of this inner ionization channel, which becomes important for large Xe_n clusters at moderately low intensities ($I_M=10^{15}-10^{16}$ W cm^{-2}) and long pulse lengths ($\tau=100$ fs). The time dependence of $n_{\mathrm{imp}}(t)$ and the EII level per Xe atom show a temporal delay relative to the $n_{\mathrm{BSI}}(t)$ curves at the same cluster size and laser intensity (Fig. 5), exhibiting the sequential nature of BSI and EII. At lower intensities of $I_M=10^{15}-10^{16}$ W cm^{-2}, EII contributes substantially to the inner ionization level n_{ii}, while this contribution decreases with increasing I_M. Figure 6 presents the simulation results for the cluster size dependence of the long-time relative impact ionization yield $n^L_{\mathrm{imp}}/n^L_{\mathrm{ii}}$ (for $\tau=25$ fs). Over the entire intensity range, the fraction of impact ionization increases monotonously with increasing R_0. As already noted, the $n^L_{\mathrm{imp}}/n^L_{\mathrm{ii}}$ fraction of inner ionization for a fixed cluster size increases with decreasing I_M. For Xe_{2171} interacting with a pulse length of 25 fs, this inner ionization fraction reaches 37% at $I_M=10^{15}$ W cm^{-2} and decreases to 6% at $I_M=10^{20}$ W cm^{-2} (Fig. 6). In order to assess the net effect of EII on the inner ionization level, we portray in Fig. 5 results for n_{ii} in a model system where the EII channel was

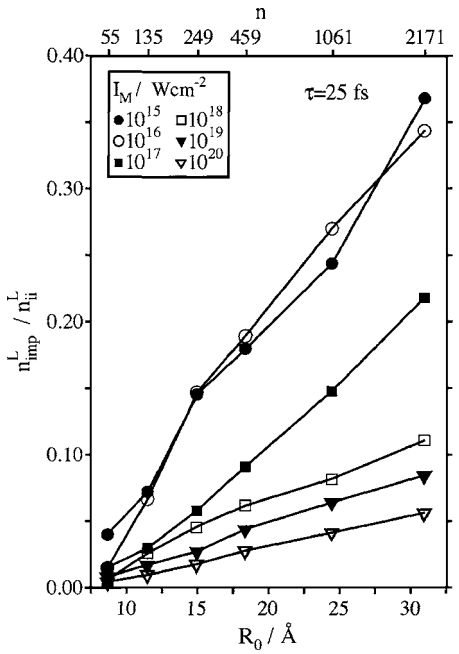

FIG. 6. The cluster size dependence of the relative EII yield n^L_{imp}/n^L_{ii} for $Xe_n(n=55-2171)$ clusters in the intensity range $I_M=10^{15}-10^{20}$ W cm^{-2} ($\tau=25$ fs).

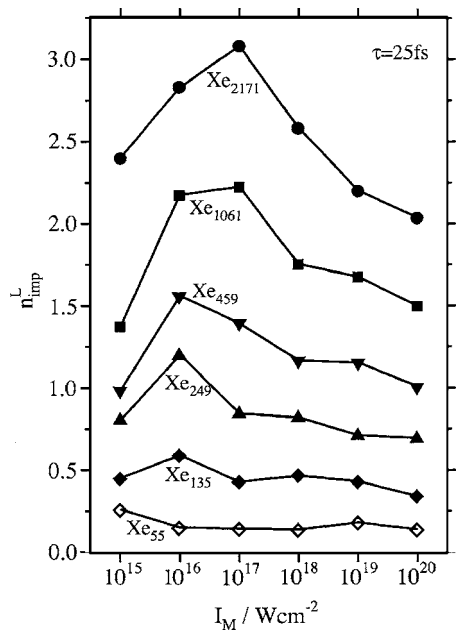

FIG. 7. The cluster size and laser intensity dependence of the long-time EII level n^L_{imp} for $Xe_n(n=55-2171)$ clusters in the intensity range $I_M=10^{15}-10^{20}$ W cm^{-2} ($\tau=25$ fs).

switched off [which is denoted as n_{ii}(no EII)]. The net effect of EII on the inner ionization was assessed from the parameter $\delta_{EII}=n^L_{ii}-n^L_{ii}$(no EII), which markedly decreases with increasing I_M. For Xe_{2171} (and $\tau=25$ fs), the δ_{EII} values are 1.74, 1.52, 0.68, and ~0 for 10^{15}, 10^{16}, 10^{17}, and 10^{18} W cm^{-2}, respectively. Accordingly, at 10^{15} W cm^{-2}, $\delta E_{EII}=1.74$ out of $n^L_{imp}\equiv 2.40$ e/at. lead to a substantial net increase of the average ion charge. At 10^{18} W cm^{-2}, the value of $\delta_{EII}\sim 0$, while $n^L_{imp}=2.59$ e/at., indicates that EII is merely a competing ionization channel in this high intensity domain.

The cluster size dependence of n^L_{imp} (Fig. 7) reveals an increase of n^L_{imp} with increasing the cluster size at fixed I_M, as expected. The contribution of EII is unimportant for $n\leqslant 55$, in accord with previous results.[14,70] Regarding the laser intensity dependence at fixed n, n^L_{imp} exhibits a maximum (for $n\geqslant 135$) around $I_M=10^{16}-10^{17}$ W cm^{-2} and a subsequent decrease with increasing I_M (Fig. 7). This intensity dependence originates from the interplay between opposing effects with the increase of I_M, resulting in the increase of the number of electrons by BSI, the decrease of the number of the nanoplasma electrons by outer ionization,[2,3,10,11,21,22,85] the "dilution" of the nanoplasma by Coulomb explosion,[86] and the production of higher kinetic energy nanoplasma electrons with smaller impact ionization cross sections. At present, we did not attempt to present a quantitative analysis of these competing effects on the cluster size dependence of n^L_{imp}.

Of interest is the effect of EII on the distribution of the Xe^{q+} ion charges. In Fig. 8 we present the long-time charge distribution $n^L(q)$ for Xe_{2171} at $I_M=10^{15}$ W cm^{-2}, where the relative yield of inner ionization is nearly maximal. Simulations were performed for laser pulse lengths $\tau=25$, 50, and 100 fs. We compare these distributions $n^L(q)$ with the corresponding data where the EII was switched off (marked as "no EII" panels in Fig. 8). In general, the effects of EII manifest the shift of the distribution $n(q)$ toward higher values of q (Fig. 8). These results exhibit a dramatic effect of EII on the upward shift of $n^L(q)$ toward higher values of q (Fig. 8), e.g., for $\tau=25$ fs, $n^L(q)$ exhibits $q_{av}=6.5$ with $q_{max}=9$, while in the absence of EII $q_{av}=4$. Increasing the pulse length results in the shift of q_{av} toward higher values, e.g.,

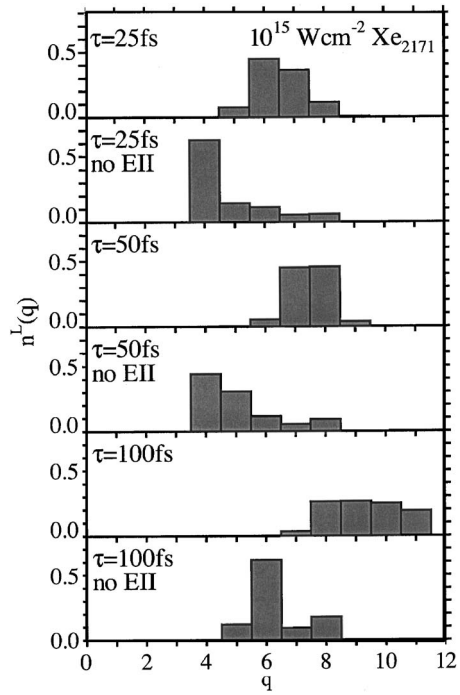

FIG. 8. The effects of EII on the long-time distribution of the Xe^{q+} ion charges. Panels 1, 3, and 5 (from top) represent full simulation results for Xe_{2171} clusters at $I_M=10^{15}$ W cm^{-2} ($\tau=25$, 50, and 100 fs). The panels marked "no EII" present simulation results for a model system where the EII channel was switched off.

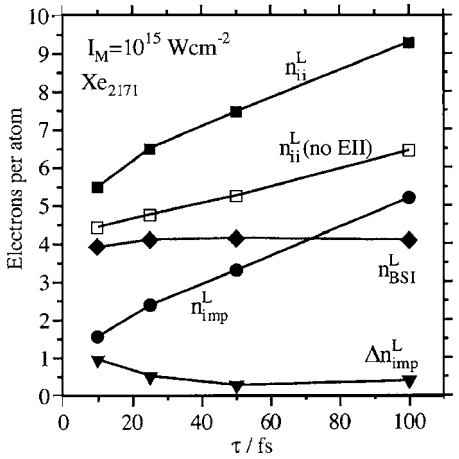

FIG. 9. The laser pulse length dependence of the long-time ionization levels of Xe_{2171} coupled to a laser field at $I_M=10^{15}$ W cm^{-2} ($\tau=10-100$ fs). Ionization levels are presented for BSI (n_{BSI}^L: ♦), for EII (n_{imp}^L: ●), for inner ionization (n_{ii}^L: ■), for inner ionization with the EII channel switched off [n_{ii}^L (no EII): □] and for "laser-free" EII (Δ_{imp}^L: ▼) in the time domain after the termination of the laser pulse. The marked increase of the inner ionization yield with increasing τ marks control by laser pulse shaping.

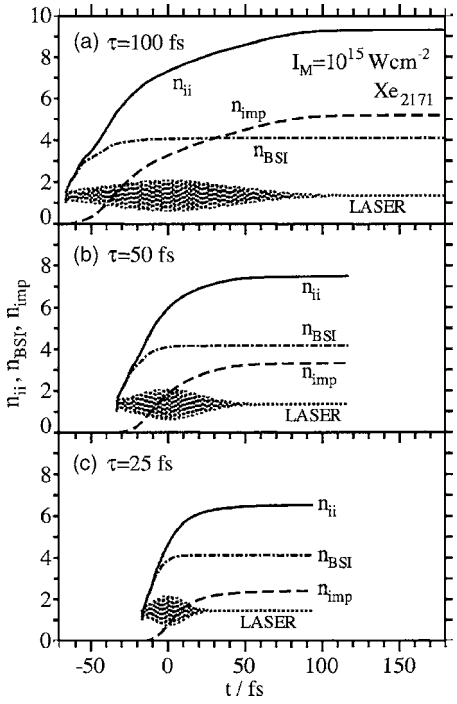

FIG. 10. Laser pulse length dependence of time-resolved inner ionization, BSI, and EII levels for Xe_{2171} clusters at $I_M=10^{15}$ W cm^{-2} ($\tau=25$, 50, and 100 fs). The laser field (⋯) is presented in arbitrary units and marked LASER.

$q_{av}=6.5$ at $\tau=25$ fs and $q_{av}=9.3$ at 100 fs. This marked increase of the higher charges of the Xe^{q+} ions with increasing τ (i.e., for $\tau=100$ fs, $q_{max}=11$, while $q_{max}=9$ in the absence of EII) reflects on significant EII effects for long pulses in the low I_M domain.

EII yields are markedly enhanced by increasing the laser pulse length. In Fig. 9 we present the laser pulse length dependence (in the range $\tau=10-100$ fs) of the long-time ionization levels of Xe_{2171} clusters coupled to a laser field at $I_M=10^{15}$ W cm^{-2}, portraying the yield for total inner ionization (n_{ii}^L), BSI (n_{BSI}^L), and EII (n_{imp}^L). BSI exhibits a weak pulse length dependence with $n_{BSI}^L=3.8-4$ over the entire range of τ. In contrast, the EII yield exhibits a strong pulse length dependence, increasing with increasing τ, i.e., from $n_{imp}^L=1.5$ at $\tau=10$ fs to $n_{imp}^L=5.2$ at $\tau=100$ fs (Fig. 9). For the longest pulse length $\tau=100$ fs studied herein $n_{imp}^L>n_{BSI}^L$ (Fig. 9), where 56% of inner ionization originates from EII, which becomes the dominant inner ionization channel for Xe_{2171} at $I_M=10^{15}$ W cm^{-2}. Our results for the dominance of EII in the lower intensity domain and for long τ are in accord with previous results[70] on a significant (20%–60%) EII contribution to n_{ii}^L in moderately large Xe_n clusters ($R_0=20-50$ Å) driven by near-infrared laser pulses at $I_M=10^{16}$ W cm^{-2} with $\tau=75$ fs. From the radial distribution of the ion charges for $I_M=10^{15}$ W cm^{-2} and $\tau=100$ fs [central panels in Figs. 4(a) and 4(b)], we infer that EII is most effective near the cluster center. The marked increase of n_{imp}^L with increasing τ at fixed $I_M=10^{15}$ W cm^{-2} also implies that the total inner ionization yield n_{ii}^L increases with increasing τ (Fig. 9). In a model system where the EII channel is switched off, a moderate increase of n_{ii}^L from 4.5 to 6.5 is exhibited with τ increasing in the range of 10–100 fs. This effect, in conjunction with the data of Fig. 9, where EII is included (and where $n_{ii}^L=9.3$ at $\tau=100$ fs), manifests the competition between BSI and EII, while EII makes the major contribution to inner ionization.

The time-resolved data for $n_{imp}(t)$ and $n_{BSI}(t)$ in Fig. 10 indicate that EII occurs sequentially to BSI (see also Sec. II). Most of the enhancement of the EII yield with increasing the laser pulse length occurs during the duration of the pulse, with $n_{imp}(t)$ reaching near (but incomplete) saturation for $t>-t_s$ (Fig. 10). This interesting feature of electron dynamics pertains to 'laser-free' EII after the termination of the laser pulse. In Fig. 9 we also portray the values of the EII enhancement after $t>-t_s$, which is given by $\Delta n_{imp}^L=n_{imp}^L-n_{imp}(-t_s)$. For Xe_{2171} at $I_M=10^{15}$ W cm^{-2}, Δn_{imp} decreases in the range of 1.0–0.3 (i.e., with 2000–600 electrons produced per pulse) in the region $\tau=10-100$ fs. The finite values of Δn_{imp} imply that EII (with a modest contribution of ~10%–20%) can be induced by the energetic persistent nanoplasma electrons in the laser-free domain.

IV. COMPARISON WITH EXPERIMENT

We now provide a comparison between our simulation results and experimental data for ionization levels of Xe_n clusters in ultraintense fields. Some experimental data[15,25,69] in the lower intensity range of $I_M=10^{11}-10^{14}$ W cm^{-2} are outside the scope of our computational and theoretical models and have to be analyzed by an extended theory which includes tunneling effects.[84] We shall limit ourselves to the intensity range of $I_M\geqslant 10^{15}$ W cm^{-2} for the analysis of experimental data[25,66,87,88] obtained using pulse widths of $\tau=20-100$ fs, which can be compared with our simulation results with a Gaussian pulse shape. We shall confront our simulation results for the maximal ionic charge q_{max} and the average ionic charge $q_{av}\equiv n_{ii}^L$ with experimental reality. Lezius *et al.*[87] reported the production of Xe^{q+} ions with a maximal charge of $q_{max}=25$ from Xe_n ($n=2\times10^6$, R_0

=270 Å) at $I_M=5\times10^{17}$ W cm^{-2}. This experimental result corresponds to $R_0 \gg R_0^{(I)} \simeq 30$ Å, where $R_0^{(I)}$ is the border radius for cluster outer ionization at the intensity of I_M.[23,24,89] Complete outer ionization prevails for $R_0 \lesssim R_0^{(I)}$, while for $R_0 > R_0^{(I)}$ a persistent (positively charged) nanoplasma exists within the cluster after the termination of the laser pulse.[23,24,32] The experimental data of Lezius *et al.*[87] correspond to the nanoplasma being persistent, allowing for the comparison with computational results for considerably smaller clusters with $R_0 \simeq R_0^{(I)}$ (with a size $n^{(I)} \simeq 2500$) at this high intensity.[32] This experimental result [87] is in accord with the simulation results which give for Xe_{2171} $q_{av}=23$ and $q_{max}=26$ at $I_M=10^{18}$ W cm^{-2}. A more direct comparison between computational and experimental results in the higher intensity range is obtained from the observations of Fukuda *et al.*,[88] who reported the production of Xe^{q+} ions with a maximal charge $q_{max}=18$ and an average charge $q_{av}=12$ from Xe_n ($n=5.5\times10^4$) clusters at $I_M=2\times10^{17}$ W cm^{-2} and $\tau=20$ fs. Our computational results for Xe_{2171} clusters at $I_M=10^{17}$ W cm^{-2} ($\tau=25$ fs) give $q_{max}=18$ and $q_{av}=14$, which is in good agreement with experiment.[88] For Xe_n ($n=10^5-10^6$, $R_0=100-210$ Å) at $I_M=2\times10^{18}$ W cm^{-2}, ionic charges are produced[66] in the ranges $q=9-11$, 13–17, and 22–30. Again, we expect that for this experimental cluster size domain $R_0 \gg R_0^{(I)}=38$ Å, allowing for the approximate comparison of the ionization levels with the computational results for a Xe_{2171} cluster [with $R_0 \lesssim R_0^{(I)}$]. At $I_M=10^{18}$ W cm^{-2} the computational results show the production of ions with $q_{av}=23$ and $q_{max}=26$ for Xe_{2171} clusters, in accord with experiment.[66] The production of higher charges ($q=26-30$) [Ref. 65] in these huge clusters ($R_0=100-200$ Å) may be due to ignition effects. A marked pulse length dependence of the ionization levels q_{av} and q_{max} of $\{Xe^{q+}\}$ is expected to be manifested for $I_M=10^{15}-10^{16}$ W cm^{-2} due to EII effects (Fig. 8). For Xe_{2171} at $I_M=10^{15}$ W cm^{-2} and $\tau=100$ fs, we predict that $q_{max}=11$, in accordance with the experimental result of $q_{max}=11$ reported by Zamith *et al.*[25] for Xe_n ($n=1.6\times10^4$) clusters at $I_M=10^{15}$ W cm^{-2} and $\tau=100$ fs. Our computational results account for the laser intensity dependence of the cluster ionization levels of Xe_n clusters.[25,66,87,88] Nevertheless, some experimental results from the 1990s (Refs. 3, 62, and 90) require further theoretical scrutiny and experimental reexamination. Several groups reported on the production of very high Xe^{q+} average and maximal charges in the lower ultraintense domain, i.e., $q_{av}=20$ at $I_M=10^{15}$ W cm^{-2} (Ref. 90) and $q_{max}=35$ at $I_M=2\times10^{16}$ W cm^{-2}.[3,62] These ionic charges are considerably higher than those predicted by our simulations in this intensity domain,[91] i.e., according to our simulation charges of $q=36$ can be produced only at $I_M=10^{20}$ W cm^{-2} (Sec. II C). The discrepancy between experiment[3,62,90] and our computational results can be explained, at least partially, by the inhomogeneity of the laser focus volume in these experiments.[92] It should also be noted that the simulated ionization levels were obtained for a single cluster size, while the experimental data correspond to the distribution of cluster sizes,[92,93] which have to be accounted for in a complete treatment.

V. CONCLUDING REMARKS

We applied theoretical models for BSI, and for experimental cross sections for EII, together with molecular dynamics simulations, to explore cluster ionization levels, which are amenable to experimental studies. The analysis of the (time-resolved) inner ionization levels of Xe_n clusters manifests some unique features.

(i) The cluster size dependence of inner ionization levels are induced by a complex superposition of laser-induced BSI, inner field ignition effects, and nanoplasma screening effects, as well as by the contribution of EII. The inner field ignition and screening effects, in conjunction with EII, constitute collective effects, which preclude the description of cluster inner ionization in terms of an additive contribution of the constituents.

(ii) The extension of the laser intensities into the relativistic domain ($I_M \geqslant 10^{18}$ W cm^{-2}) allowed for bridging between the high intensity range of $I_M=10^{18}-10^{20}$ W cm^{-2}, where BSI is dominant, and the laser intensity range of $I_M=10^{15}-10^{16}$ W cm^{-2}, where EII is important.

(iii) EII manifests a pronounced effect on the inner ionization levels of Xe_n clusters ($n>55$) at moderate intensities ($I_M=10^{15}-10^{16}$ W cm^{-2}). EII is important for clusters of heavy multielectron atoms or molecules, e.g., Xe_n, where the corresponding cross sections are large.[29,75] The treatment of EII presented herein considered only outer shell ionization of ions. For electrons with sufficiently high kinetic energies (e.g., from our simulations we infer that the average nanoplasma electron energies are 0.93 keV at $I_M=10^{17}$ W cm^{-2} and 72 keV at $I_M=10^{18}$ W cm^{-2}), inner shell impact ionization (ISII) becomes important for large clusters ($n>10^5$).[3,94] At high intensities ($I_M>10^{17}$ W cm^{-2}) the nanoplasma electrons are accelerated to high energies and the energetics for ISII will be effective. However, the transient nature of the nanoplasma at these high intensities[22,85] will reduce the ISII yield. Significantly, in the persistent nanoplasma domain (at $I_M=10^{15}-10^{16}$ W cm^{-2}), the EII yields and the values of $q_{av}=n_{ii}^L$ and q_{max} manifest a marked increase with increasing the laser pulse length. Another interesting effect pertains to 'laser-free' EII by the persistent nanoplasma (with a modest yield of 10%–20%), which was documented. On the other hand, at higher intensities ($I_M>10^{17}$ W cm^{-2}), where outer ionization is complete and the nanoplasma is transient being characterized by a high energy ($\geqslant 1$ keV), the cross sections for EII are reduced.[75] EII competes with BSI, but does not lead to a marked net effect on the inner ionization levels.

(iv) EII dynamics opens avenues for the control of reaction products from clusters in ultraintense laser fields. In this context, Vrakking *et al.*[25,26] advanced and investigated optimal control of the ionization level of Xe_n clusters by the shaping of a laser pulse train (at $I_M=10^{14}$ W cm^{-2}). The dependence of the inner ion-

ization level on the pulse length, with $q_{\mathrm{av}}(=n_{\mathrm{ii}}^{L})$ for Xe_{2171} at $I_M=10^{15}$ W cm^{-2} increasing from $q_{\mathrm{av}}=5.5$ at $\tau=10$ fs to $q_{\mathrm{av}}=9.3$ at $\tau=100$ fs (Fig. 9), constitutes control of extreme ionization in ultraintense laser fields, which is driven by EII in the persistent nanoplasma.

ACKNOWLEDGMENTS

This research was supported by the Deutsche Forschungsgemeinschaft (DFG) SFB 450 on "Analysis and Control of Ultrafast Photoinduced Reactions" and by the James-Franck Binational German-Israeli Program on Laser-Matter Interaction.

[1] A. W. Castleman and P. Jena, Proc. Natl. Acad. Sci. U.S.A. **103**, 10552 (2006).
[2] V. P. Krainov and M. B. Smirnov, Phys. Rep. **370**, 237 (2002).
[3] U. Saalmann, Ch. Siedschlag, and J. M. Rost, J. Phys. B **39**, R39 (2006).
[4] T. Ditmire, T. Donnely, A. M. Rubenchik, R. W. Falcone, and M. D. Perry, Phys. Rev. A **53**, 3379 (1996).
[5] T. Ditmire, J. W. G. Tisch, E. Springate, M. B. Mason, N. Hay, R. A. Smith, J. Marangos, and M. H. R. Hutchinson, Nature (London) **386**, 54 (1997).
[6] T. Ditmire, Phys. Rev. A **57**, R4094 (1998).
[7] J. Liu, R. Li, P. Zhu, Zh. Xu, and J. Liu, Phys. Rev. A **64**, 033426 (2001).
[8] P. B. Parks, T. E. Cowan, R. B. Stephens, and E. M. Campbell, Phys. Rev. A **63**, 063203 (2001).
[9] V. P. Krainov and A. S. Roshchupkin, J. Phys. B **34**, L297 (2001).
[10] I. Last and J. Jortner, Phys. Rev. A **62**, 013201 (2000).
[11] I. Last and J. Jortner, Phys. Rev. A **64**, 063201 (2001).
[12] U. Saalmann and J. M. Rost, Phys. Rev. Lett. **89**, 143401 (2002).
[13] M. Lezius, V. Blanchet, M. Yu. Ivanov, and A. Stolow, J. Chem. Phys. **117**, 1575 (2002).
[14] D. Bauer and A. Macchi, Phys. Rev. A **68**, 033201 (2003).
[15] J. Schulz, H. Wabnitz, T. Laarmann, S. Gürtler, W. Laasch, A. Swiderski, Th. Möller, and A. A. B. de Castro, Nucl. Instrum. Methods Phys. Res. A **507**, 572 (2003).
[16] Ch. Siedschlag and J.-M. Rost, Phys. Rev. Lett. **89**, 173401 (2002).
[17] Ch. Siedschlag and J.-M. Rost, Phys. Rev. Lett. **93**, 043402 (2004); Phys. Rev. A **71**, 031401 (2004).
[18] C. Jungereuthmayer, L. Ramunno, J. Zanghellini, and T. Brabec, J. Phys. B **38**, 3029 (2005).
[19] T. Laarman, A. R. B. De Castro, P. Gürtler, W. Laasch, J. Schulz, H. Wabnitz, and T. Möller, Phys. Rev. Lett. **92**, 143401 (2004).
[20] K. W. Madison, P. K. Patel, D. Price, A. Edens, M. Allen, T. E. Cowan, J. Zweiback, and T. Ditmire, Phys. Plasmas **11**, 270 (2004).
[21] I. Last and J. Jortner, J. Chem. Phys. **120**, 1336 (2004).
[22] I. Last and J. Jortner, J. Chem. Phys. **120**, 1348 (2004).
[23] I. Last and J. Jortner, J. Chem. Phys. **121**, 3030 (2004).
[24] I. Last and J. Jortner, J. Chem. Phys. **121**, 8329 (2004).
[25] S. Zamith, T. Martchenko, Y. Ni, S. A. Aseyev, H. G. Muller, and M. J. J. Vrakking, Phys. Rev. A **70**, 011201(R) (2004).
[26] T. Martchenko, Ch. Siedschlag, S. Zamith, H. G. Muller, and M. J. J. Vrakking, Phys. Rev. A **72**, 053202 (2005).
[27] S. Ter-Avetisyan, M. Schnürer, D. Hilscher, U. Jahnke, S. Busch, P. V. Nickles, and W. Sandner, Phys. Plasmas **12**, 012702 (2005).
[28] D. Niu, H. Li, F. Liang, L. Wen, X. Luo, B. Wang, and H. Qu, J. Chem. Phys. **122**, 151103 (2005).
[29] A. Heidenreich, I. Last, and J. Jortner, Eur. Phys. J. D **35**, 567 (2005).
[30] M. Hohenberger, D. R. Symes, K. W. Madison, A. Sumeruk, G. Dyer, A. Edens, W. Grigsby, G. Hays, M. Teichmann, and T. Ditmire, Phys. Rev. Lett. **95**, 195003 (2005).
[31] S. Ter-Avetisyan, M. Schnürer, P. V. Nickles, M. Kalashnikov, E. Risse, T. Sokollik, W. Sandner, A. Andreev, and V. Tikhonchuk, Phys. Rev. Lett. **96**, 145006 (2006).
[32] I. Last and J. Jortner, Phys. Rev. A **73**, 013202 (2006).
[33] Ch. Siedschlag and J. M. Rost, Phys. Rev. A **67**, 13404 (2003).
[34] V. Kumarappan, M. Krishnamurthy, and D. Mathur, Phys. Rev. A **67**, 063207 (2003).
[35] E. Springate, S. A. Aseyev, S. Zamith, and M. J. J. Vrakking, Phys. Rev. A **68**, 053201 (2003).
[36] M. Rusek and A. Orlowski, Phys. Rev. A **71**, 043202 (2005).
[37] M. Krishnamurthy, D. Mathur, and V. Kumarappan, Phys. Rev. A **69**, 033202 (2004).
[38] G. M. Petrov and J. Davis, Phys. Plasmas **13**, 033106 (2006).
[39] J. Liu, Ch. Wang, B. Liu, B. Shuai, W. Wang, Y. Cai, H. Li, G. Ni, R. Li, and Z. Xu, Phys. Rev. A **73**, 033201 (2006).
[40] M. Hirokane, S. Shimizu, M. Hashida, S. Okada, S. Okihara, F. Sato, T. Iida, and S. Sakabe, Phys. Rev. A **69**, 063201 (2004).
[41] S. Sakabe, S. Shimizu, M. Hashida*et al.*, Phys. Rev. A **69**, 023203 (2004).
[42] J. Zweiback, T. E. Cowan, R. A. Smith, J. H. Hartlay, R. Howell, C. A. Steinke, G. Hays, K. B. Wharton, J. K. Crane, and T. Ditmire, Phys. Rev. Lett. **85**, 3640 (2000).
[43] J. Zweiback, T. E. Cowan, J. H. Hartley, R. Howell, K. B. Wharton, J. K. Crane, V. P. Yanovski, G. Hays, R. A. Smith, and T. Ditmire, Phys. Plasmas **9**, 3108 (2002).
[44] K. W. Madison, P. K. Patel, M. Allen, D. Price, R. Fitzpatrick, and T. Ditmire, Phys. Rev. A **70**, 053201 (2004).
[45] M. Isla and J. A. Alonso, Phys. Rev. A **72**, 023201 (2005).
[46] T. E. Dermota, D. P. Hydutsky, N. J. Bianco, and A. W. Castleman, Jr., J. Chem. Phys. **123**, 214308 (2005).
[47] G. Grillon, Ph. Balcou, J.-P. Chambaret *et al.*, Phys. Rev. Lett. **89**, 065005 (2002).
[48] J. Purnell, E. M. Snyder, S. Wei, and A. W. Castleman, Jr., Chem. Phys. Lett. **229**, 333 (1994).
[49] J. W. G. Tisch, N. Hay, E. Springate, E. T. Gumbrell, M. H. R. Hutchinson, and J. P. Marangos, Phys. Rev. A **60**, 3076 (1999).
[50] M. Eloy, R. Azambuja, T. M. Mendonca, and R. Bingham, Phys. Plasmas **8**, 1084 (2001).
[51] E. S. Toma and H. G. Muller, Phys. Rev. A **66**, 013204 (2002).
[52] Y. Fukuda, K. Yamakawa, Y. Akahane, M. Aoyama, N. Inoue, H. Ueda, and Y. Kishimoto, Phys. Rev. A **67**, 061201(R) (2003).
[53] Ch. Siedschlag and J. M. Rost, Phys. Rev. A **71**, 031401(R) (2005).
[54] V. Mijoule, L. J. Lewis, and M. Meunier, Phys. Rev. A **73**, 033203 (2006).
[55] S. V. Fomichev, S. V. Popruzhenko, D. F. Zaretsky, and W. Becker, J. Phys. B **36**, 3817 (2003).
[56] P. Mulser, M. Kanapathipillai, and D. H. H. Hoffmann, Phys. Rev. Lett. **95**, 103401 (2005).
[57] M. Kundu and D. Bauer, Phys. Rev. Lett. **96**, 123401 (2006).
[58] Ch. Jungreuthmayer, M. Geissler, J. Zanghellini, and T. Brabec, Phys. Rev. Lett. **92**, 133401 (2004).
[59] I. Last and J. Jortner, Phys. Rev. A **73**, 063201 (2006).
[60] S. Augst, D. Strickland, D. D. Meyerhofer, S. L. Chin, and J. H. Eberly, Phys. Rev. Lett. **63**, 2212 (1989).
[61] M. Schnürer, S. Ter-Avetisyan, H. Stiel, U. Vogt, W. Radloff, M. Kalashnikov, W. Sandner, and P. V. Nickles, Eur. Phys. J. D **14**, 331 (2001).
[62] T. Ditmire, E. Springate, J. W. G. Tisch, Y. L. Shao, M. B. Mason, N. Hay, J. P. Marangos, and M. H. R. Hutchinson, Phys. Rev. A **57**, 369 (1998).
[63] E. Springate, N. Hay, J. W. G. Tisch, M. B. Mason, T. Ditmire, M. H. R. Hutchinson, and J. P. Marangos, Phys. Rev. A **61**, 063201 (2000).
[64] K. J. Mendham, N. Hay, M. B. Mason, J. W. G. Tisch, and J. P. Marangos, Phys. Rev. A **64**, 055201 (2001).
[65] S. Ter-Avetisyan, M. Schnürer, H. Stiel, U. Vogt, W. Radloff, W. Karpov, W. Sandner, and P. V. Nickels, Phys. Rev. E **64**, 036404 (2001).
[66] P. V. Nickles, S. Ter-Avetisyan, H. Stiel, W. Sander, and M. Schnürer, AIP Conf. Proc. (2002), p. 611.
[67] W. Wabnitz, L. Bittner, A. R. B. de Castro *et al.*, Nature (London) **420**, 481 (2002).
[68] V. Kumarappan, M. Krishnamurthy, and D. Mathur, Phys. Rev. A **66**, 033203 (2002).
[69] X. Luo, H. Li, D. Niu, L. Wen, F. Liang, and X. Xiao, Phys. Rev. A **72**, 013201 (2005).
[70] G. M. Petrov, J. Davis, A. L. Velikovich, P. Kepple, A. Dasgupta, and R. W. Clark, Phys. Plasmas **12**, 063103 (2005).
[71] G. M. Petrov and J. Davis, Phys. Plasmas **13**, 033106 (2006).
[72] R. Santra and Ch. H. Greene, Phys. Rev. Lett. **91**, 233401 (2003).
[73] F. Megi, M. Belkacem, M. A. Bouchene, E. Suraud, and G. Zwicknagel, J. Phys. B **36**, 273 (2003).
[74] W. Lotz, Z. Phys. **216**, 241 (1968).
[75] C. Achenbach, A. Müller, E. Salzborn, and R. Becker, J. Phys. B **17**,

1405 (1984); D. C. Griffin, C. Bottcher, M. S. Pindzola, S. M. Younger, D. C. Gregory, and D. H. Crandall, Phys. Rev. A **29**, 1729 (1984); **27**, 2338 (1983); M. E. Bannister, D. W. Mueller, L. J. Wang, M. S. Pindzola, D. C. Griffin, and D. C. Gregory, *ibid.* **38**, 38 (1988); G. Hofmann, J. Neumann, U. Pracht, K. Tinschert, M. Stenke, R. Völper, A. Müller, and E. Salzborn, AIP Conf. Proc. **274**, 485 (1993).
[76] C. Rose-Petruck, K. J. Schafer, K. R. Wilson, and C. P. J. Barty, Phys. Rev. A **55**, 1182 (1997).
[77] T. Zuo and A. D. Bandrauk, Phys. Rev. A **52**, R2511 (1995).
[78] T. Seideman, M. Yu. Ivanov, and P. B. Corkum, Phys. Rev. Lett. **75**, 2819 (1995).
[79] T. Seideman, M. Yu. Ivanov, and P. B. Corkum, Chem. Phys. Lett. **252**, 181 (1996).
[80] P. B. Corkum, Phys. Rev. Lett. **71**, 1994 (1993).
[81] F. Krausz, Opt. Photonics News **13**, 62 (2002).
[82] S. Niikma, F. Légaré, R. Habashi, A. D. Bandrauk, M. Y. Ivanov, D. M. Villeneuve, and P. B. Corkum, Nature (London) **417**, 917 (2002).
[83] V. E. Bhardwaj, P. B. Corkum, and D. M. Rayner, Phys. Rev. Lett. **93**, 5400 (2005).
[84] M. V. Amossov, N. B. Delone, and V. P. Krainov, Sov. Phys. JETP **64**, 1191 (1986).
[85] A. Heidenreich, I. Last, and J. Jortner (unpublished).
[86] A. Heidenreich, I. Last, and J. Jortner (unpublished).
[87] M. Lezius, S. Dobosz, D. Normand, and M. Schmidt, Phys. Rev. Lett. **80**, 261 (1998).
[88] Y. Fukuda, K. Yomakawa, Y. Akahane, M. Ayomaya, N. Inoue, H. Ueda, and Y. Kishimoto, Phys. Rev. A **67**, 061201(R) (2003).
[89] The border radius $R_0^{(I)}$ was denoted in Refs. 23 and 24 as $(R_0)_I$.
[90] E. M. Snyder, S. A. Buzza, and A. W. Castleman, Jr., Phys. Rev. Lett. **77**, 3347 (1996).
[91] I. Last and J. Jortner, Phys. Rev. A **73**, 063201 (2006).
[92] M. R. Islam, U. Saalmann, and J. M. Rost, Phys. Rev. A **73**, 041201 (2006).
[93] K. W. Madison, P. K. Patel, D. Price, A. Edems, M. Allen, T. E. Cowan, J. Zweiback, and T. Ditmire, Phys. Plasmas **11**, 270 (2004); K. J. Mendham, N. Hay, M. B. Mason, J. W. G. Tisch, and J. P. Marangos, Phys. Rev. A **64**, 055201 (2001).
[94] C. Deiss, N. Rohringer, J. Burgdörfer, E. Lamour, C. Prigent, J.-P. Rozet, and D. Vernhet, Phys. Rev. Lett. **96**, 013203 (2006).